Title

Animals deficient in C2Orf71, an autosomal recessive retinitis pigmentosa-associated locus, develop severe early-onset retinal degeneration.

Journal

Human Molecular Genetics, 24(9)

Authors

Kevany, Brian
Zhang, Ning
Jastrzebska, Beata
et al.

Publication Date

2015-05-01

DOI

10.1093/hmg/ddv025

Peer reviewed

Human Molecular Genetics, 2015, Vol. 24, No. 9 2627–2640

doi: 10.1093/hmg/ddv025
Advance Access Publication Date: 23 January 2015
Original Article

ORIGINAL ARTICLE

Animals deficient in C2Orf71, an autosomal recessive retinitis pigmentosa-associated locus, develop severe early-onset retinal degeneration

Brian M. Kevany, Ning Zhang, Beata Jastrzebska and Krzysztof Palczewski*

Department of Pharmacology, Cleveland Center for Membrane and Structural Biology, School of Medicine, Case Western Reserve University, Cleveland, OH 44106, USA

*To whom correspondence should be addressed at: Department of Pharmacology, School of Medicine, Case Western Reserve University, 10900 Euclid Ave, Cleveland, OH 44106-4965, USA. Tel: +1 216368 4631; Fax: +1 2163681300; Email: kxp65@case.edu

Abstract

Genetic mapping was recently used to identify the underlying cause for a previously uncharacterized cohort of autosomal recessive retinitis pigmentosa cases. Genetic mapping of affected individuals resulted in the identification of an uncharacterized gene, *C2Orf71*, as the causative locus. However, initial homology searches failed to reveal similarities to any previously characterized protein or domain. To address this issue, we characterized the mouse homolog, BC027072. Immunohistochemistry with a custom polyclonal antibody showed staining localized to the inner segments (IS) of photoreceptor cells, as well as the outer segments (OS) of cone cells. A knockout mouse line ($BC^{-/-}$) was generated and demonstrated that loss of this gene results in a severe, early-onset retinal degeneration. Histology and electron microscopy (EM) revealed disorganized OS as early as 3 weeks with complete loss by 24 weeks of age. EM micrographs displayed packets of cellular material containing OS discs or IS organelles in the OS region and abnormal retinal pigmented epithelium cells. Analyses of retinoids and rhodopsin levels showed <20% in $BC^{-/-}$ versus wild-type mice early in development. Electroretinograms demonstrated that affected mice were virtually non-responsive to light by 8 weeks of age. Lastly, RNAseq analysis of ocular gene expression in $BC^{-/-}$ mice revealed clues to the causes of the progressive retinal degenerations. Although its function remains unknown, this protein appears essential for normal OS development/maintenance and vision in humans and mice. RNAseq data are available in the GEO database under accession: GSE63810.

Introduction

Visual perception is initiated by the absorption of photons by visual pigments within the eye's retina. Consisting of the 11-*cis*-retinal chromophore attached to an opsin protein, these pigments are housed in polarized rod and cone photoreceptor cells that collect and process light data and send signals to the brain (1). There are four distinct domains within these photoreceptor cells: the synaptic terminal, outer segment (OS), inner segment (IS) and the connecting cilium which bridges the IS and OS (2). The OS is a specialized cilium which contains hundreds of either independent discs in rods, or evaginations emanating from the plasma membrane in cones. Development and maintenance of these discs and evaginations with their visual pigments and all of the phototransduction machinery is essential for sustained vision (3).

Retinitis pigmentosa (RP) is a genetically and phenotypically heterogeneous disease, with at least 48 distinct loci known to result in its pathogenesis when mutated, but those 48 only represent ~50% of clinical cases of RP (4–6). The prevalence of RP is ~1 in 4000, making it the most common form of inherited retinal dystrophy. The inheritance pattern of these genetic defects can be autosomal dominant, autosomal recessive or X-linked. Individuals diagnosed with RP present with retinal pigment

Received: December 4, 2014. **Revised:** December 31, 2014. **Accepted:** January 21, 2015

deposits, macular atrophy and night blindness leading to eventual blindness. RP-causing mutations appear in genes of diverse functions including those involving phototransduction, the visual cycle, retinal pigmented epithelium (RPE) phagocytosis, photoreceptor OS structures, retinal development and ciliary structure and maintenance (7). Non-syndromic RP is generally caused by mutations in genes that are exclusively expressed in the eye, such as those for rhodopsin, guanylate cyclase-activating protein 1 (GCAP1), RPE65 or peripherin/rds. But recently, a number of genes were identified that are the underlying causes of unknown forms of non-syndromic RP which affect the cilia of photoreceptor cell OS (8–10). These proteins co-localize with other known ciliary proteins in photoreceptor cell cilia and are believed to be involved in ciliary biogenesis and maintenance, as well as intraflagellar transport.

Homozygosity mapping and exome sequencing have revolutionized our ability to uncover pathogenic mutations causing human diseases (5,11–16). These techniques were recently used to identify the underlying molecular basis for a previously uncharacterized cohort of autosomal recessive RP cases (17,18). Affected individuals presented with typical RP symptoms including bone-spicule type retinal deposits, attenuated blood vessels, night blindness and undetectable electroretinogram (ERG) signals by the third decade of life, with some displaying symptoms during early childhood. Genetic mapping of affected individuals resulted in the identification of a previously uncharacterized gene, *C2Orf71*, as the causative locus. Affected individuals had missense mutations as well as nonsense mutations resulting in premature stop codons (11,17–22). Examination of the gene revealed an open reading frame with two exons, one of which represented 95% of the coding region. The translated product contained 1288 amino acids with a predicted molecular weight of 139 kDa. Initial homology searches failed to identify similarity to any previously characterized protein or domain, suggesting a completely novel protein (Fig. 1A). Post-translational modification searches resulted in two predicted lipid modification sites at the extreme N-terminus of the protein. The protein is predicted to be both *N*-myristoylated (at G2) (23) and palmitoylated (at C3) (24), but contains no other predictable modification sites. The protein has no canonical signal peptide, suggesting that it does not enter a secretory pathway. Expression analysis suggests that this gene is exclusively expressed in the eye, consistent with the non-syndromic symptoms of affected individuals. Knockdown of this gene in zebrafish with morpholinos resulted in thinning of the photoreceptor OS and an attenuated behavioral response to light exposure (17). Expression of this gene in mammalian cell culture localized the protein to the centrosome, a microtubule organizing center which often originates ciliary structures (17).

The absence of any primary structural information and lack of an animal model presents a significant impediment to understanding the function of this protein and its relationship to retinal disease in humans. To address this issue we set out to characterize the mouse homolog, BC027072. Here, we present an analysis of gene expression and protein localization of BC027072, as well as detailed analysis of the $BC^{-/-}$ mice.

Results

BC027072 expression analysis

Data mining as well as previous studies suggest that BC027072 is almost exclusively expressed in the eye, with a significantly lower expression found in the testes, which are known to have a relaxed chromatin structure leading to aberrant expression (25). Previous studies relied on semi-quantitative polymerase chain reaction (qRT-PCR) or microarray analysis for gene expression analyses. To provide a more thorough analysis, we used qRT-PCR to analyze gene expression in a range of mouse tissues as well as in different compartments of the eye. Our analysis confirms previous reports with the eye manifesting significantly higher expression than any other tissue (Fig. 2A) (18), with a low amount of expression found in the testes, consistent with other studies. Within the eye, expression was confined to the neural retina, with little or no expression detected in the RPE/choroid tissues (Fig. 2B). To understand the expression of this gene in the mouse eye, we mined our recently analyzed RNASeq transcriptome data from various species and tissues. In rod dominant rodents, BC027072 was expressed at levels comparable to those of ABCA4, an important component of the retinoid cycle in the retina (26) (Table 1). Comparison of expression levels across species, including those with varying numbers of rods and cones, suggests that this gene is expressed in both rod and cone photoreceptor cells.

Cellular and subcellular localization of BC027072 in photoreceptor cells

To determine its cellular and subcellular localization, we generated a polyclonal antibody (pAb) against recombinant BC027072 expressed in Sf9 insect cells. Test blots against BC027072 expressed in *Escherichia coli* displayed a clear single band. Analysis of native eye tissue from mice with our pAb yielded a distinct band of the appropriate size, which was seen only in samples that included retinal tissue (Fig. 3A). Analysis of cryosections by immunohistochemistry (IHC) revealed a photoreceptor-specific localization, with staining in the IS of both rod and cone photoreceptors and a significant level of expression in the OS of what appeared to be cone photoreceptors. Co-labeling with peanut agglutinin (PNA) or cone opsin confirmed the expression in cone OS (Fig. 3B). qRT-PCR analysis of RNA from the coneless transgenic line (27), ConeDTA, which expresses diphtheria toxin A under a cone-specific promoter, showed robust expression of BC027072, ruling out a cone-specific expression.

Early-onset retinal degeneration in $BC^{-/-}$ mice

Next, we generated a knockout mouse line by replacing exon 1 (>95% of the coding region of BC027072) with a neomycin cassette (Fig. 4A and B). Crossing $BC^{+/-}$ mice provided the expected Mendelian ratios with no apparent effect on viability. Additionally, viability appeared normal in mating pairs of two homozygous $BC^{-/-}$ mice with litter sizes comparable to those seen for mating pairs of heterozygous mice, consistent with the tissue specificity of this gene. Analysis of gene expression in the eye by qRT-PCR showed a virtually complete lack of transcripts in $BC^{-/-}$ mice (Fig. 4C). In $BC^{-/-}$ mice, outer nuclear layer (ONL) thinning could be seen as early as 4 weeks of age. As analyzed by spectral domain optical coherence tomography (SD-OCT), ONL thickness had already decreased ~25% by 4 weeks of age and rapidly degenerated further with 42 and 81% of the retina lost by 8 and 24 weeks of age, respectively (Fig. 5A and C). Histological examination of plastic-embedded tissues not only displayed thinning of the ONL but also a highly disorganized OS as compared with wild-type (WT) negative littermates. Examination of 24-week-old mice revealed a nearly complete absence of OS and ONL layers which were only two nuclei thick (Fig. 5B and D).

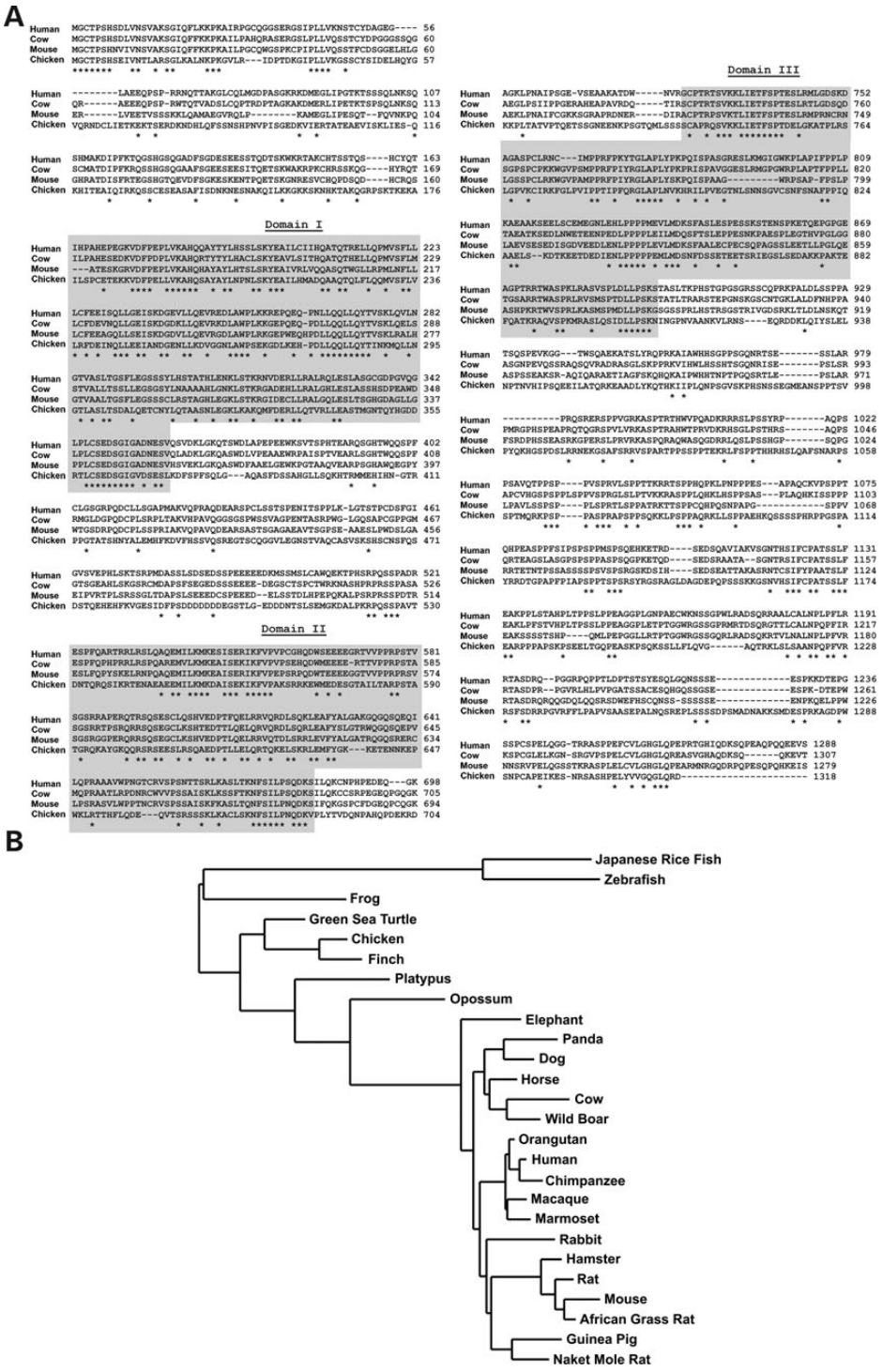

Figure 1. Sequence alignment of C2Orf71 and its homologs. (**A**) Sequences from human, cow, mouse and chicken were aligned with ClustalW alignment software. Asterisks indicate amino acids conserved in all four species. Gray-shaded areas represent domains that are potentially homologous between species and were chosen solely based on high levels of sequence identity between all four species. (**B**) Phylogenetic tree including C2Orf71 sequences from 26 species that include mammals, birds and fish.

Disorganization of OS layers is often seen in retinal degenerative mouse models but can be caused by many different mechanisms, including improper or complete lack of transport of rhodopsin to the OS. To determine whether these disorganized layers contained rhodopsin, cryosections were probed with anti-rhodopsin 1D4 antibody. Although rhodopsin was clearly transported to the OS, there remained significant staining in the IS and the ONL (Fig. 6A). This observation suggests that this degeneration is at least partly caused by deficient transport of proteins to the OS. Measurement of rhodopsin levels only

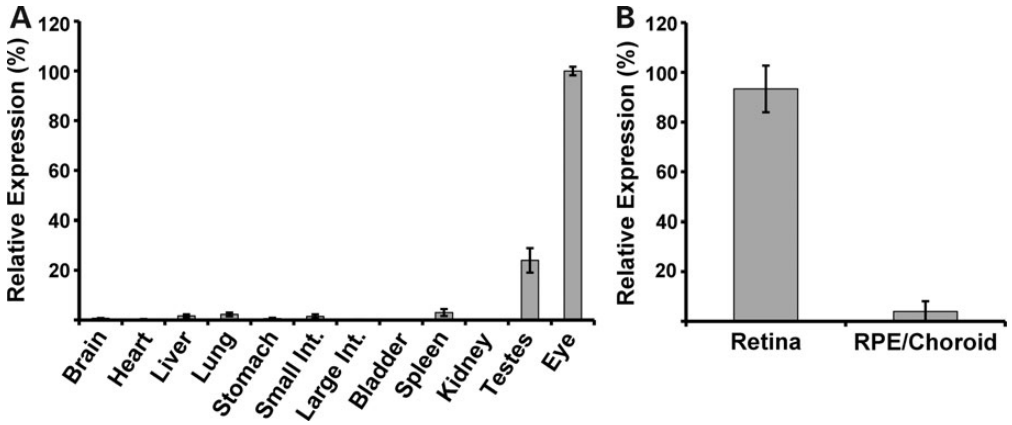

Figure 2. Gene expression analysis by qRT-PCR. Gene-specific primers/probes were used to probe gene expression in various mouse organs (**A**) or eye tissues (**B**) with Taqman quantitative real-time PCR. Results demonstrate a nearly exclusive expression in the neural retina. The 18S rRNA band was used as an internal control.

Table 1. Gene expression analysis by RNAseq

	C2Orf71	Gcap1	Abca4	Rho
Mouse eye	47.3	566.7	68.5	9113.6
Mouse retina	101.1	720.2	175.7	11745.1
$Nrl^{-/-}$ eye	33.3	508.0	20.3	0.6
$Rho^{-/-}$ eye	20.4	205.9	15.8	39.3
Rat eye	56.3	337.2	53.4	9831.1
Rat retina	99.5	685.2	124.5	21293.3
Nile rat eye	2.4	409.8	16.5	1272.5
Human retina	36.7	1140.0	267.7	6386.1

Values represented as fragments per kilobase per million (FPKM) reads.

addresses the integrity of rod photoreceptors. To analyze other important layers in the outer retina, we determined the levels of OPN1SW for cone photoreceptors and RPE65 for the RPE. IHC analyses provided what appeared to be normal staining for RPE65, but OPN1SW exhibited a reduced staining consistent with degeneration of cone OS (Fig. 6B). An additional factor that could accelerate degeneration is the activation of immune cells within the retina. Staining for microglia with Iba-1 antibody showed that activated glial cells had migrated to the outer retinas of mice by 3 weeks of age and showed a pronounced activation at later time points (Fig. 6C).

Although IHC analysis provided a qualitative assessment, we also wanted to determine what the quantitative differences were between WT and $BC^{-/-}$ mice with respect to retinoids and visual pigment. Analysis of retinoids from dark-adapted mice revealed a 78% decline in 11-*cis*-retinal in $BC^{-/-}$ relative to WT mice, 63.8 ± 0.9 pmol/eye and 277.8 ± 11 pmol/eye, respectively (Fig. 7A). Similarly, spectrophotometric analysis indicated that $BC^{-/-}$ animals contained only ~16% of the retinal pigment as did WT animals at 3 weeks of age, with 1.4 µg/retina and 8.6 µg/retina in $BC^{-/-}$ and WT, respectively (Fig. 7B). Although this clearly demonstrated a quantitative difference between WT and $BC^{-/-}$ mice, we then determined if the remaining visual pigment in $BC^{-/-}$ mice was qualitatively similar to that of WT animals. Regeneration of free opsin with 9-*cis*-retinal demonstrated that regeneration was similar between WT and $BC^{-/-}$ mice (28). Additionally, we found no difference in remaining pigment G_t activation between WT and $BC^{-/-}$ mice performed as described recently (29).

Electron microscopy reveals highly disorganized outer segments

High resolution electron microscopy (EM) permits the visualization of individual photoreceptor and RPE cells. Although well-ordered stacks of discs were seen in the OS of WT mice, $BC^{-/-}$ animals featured severe disorganization of OS morphology as early as 3 weeks of age (Fig. 8A and B). Whirls of disc membranes were seen in membranous structures surrounded by what appeared to be plasma membranes. This degeneration was so severe that packets of IS containing mitochondria could be identified immediately adjacent to the RPE cell layer at a significant distance from their normal location (Fig. 8C). Intact connecting cilia (CC) could be seen with their associated basal bodies and ciliary rootlets but none were attached to their OS (Fig. 8D). Some CCs appeared to have broken off from their IS whereas others were still attached to these structures. Additionally, RPE cells appeared to have either higher levels of pigmentation or contain large numbers of phagosomes with disc membrane material (Fig. 8F). Analysis of 8-week-old affected mice also revealed some necrotic RPE cells, possibly overwhelmed by massive retinal degeneration (Fig. 8G and H).

$BC^{-/-}$ mice display attenuated ERG responses

The presence of rhodopsin in the OS of $BC^{-/-}$ mice suggests that at least some of the phototransduction components are present. To test the retinal function of our $BC^{-/-}$ mice we performed ERG analyses on 4- and 8-week-old animals (Fig. 9A and B). Consistent with the severe structural disorganization observed, only 4 week $BC^{-/-}$ mice possessed detectable a-waves at the highest stimulus intensities. By 8 weeks of age, ERG responses were virtually flat, as opposed to a strong response in WT mice. Although discs, as well as aberrant OSs, were being produced, vision was severely compromised, even in young animals.

RNA sequencing of $BC^{-/-}$ mice reveals clues to pathophysiology

Transcriptome analysis has long been a trusted strategy to obtain a snapshot of what is happening in a tissue or cell at the transcriptional level. We used RNASeq technology to sequence every transcript being expressed in the eye of both WT and $BC^{-/-}$ mice at 3 weeks of age. This age was chosen because the photoreceptor layer had not begun to degenerate, with an ONL

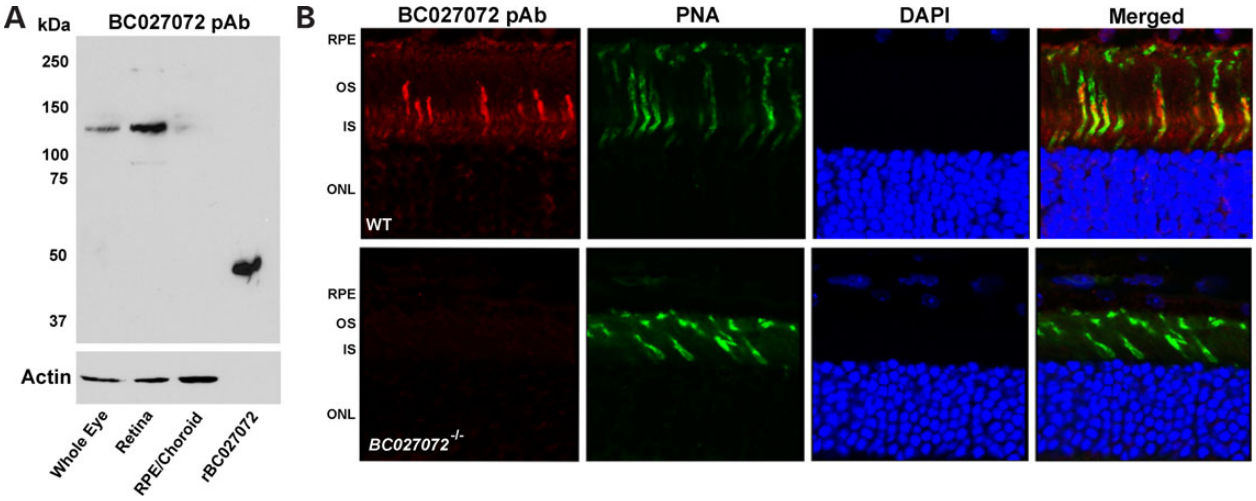

Figure 3. Immunoblot and IHC localization of BC027072 in mouse eye with a custom pAb. (**A**) Tissues were dissected and proteins were extracted with RIPA buffer. Immunoblot analysis confirmed the qRT-PCR analysis and demonstrated that expression is confined to the neural retina within the eye. rBC027072 is a truncated recombinant protein (amino acids 1–360) expressed in *E. coli* which was not used for immunization. (**B**) Eyes from 3-week-old WT and $BC^{-/-}$ mice were fixed in paraformaldehyde and embedded in OCT compound. Cryosections (12 µm) were probed with a BC027072 pAb and PNA (for cone cell staining). Staining of BC027072 is consistent with localization to the IS of both cone and rod photoreceptors as well as the OS of cone cells.

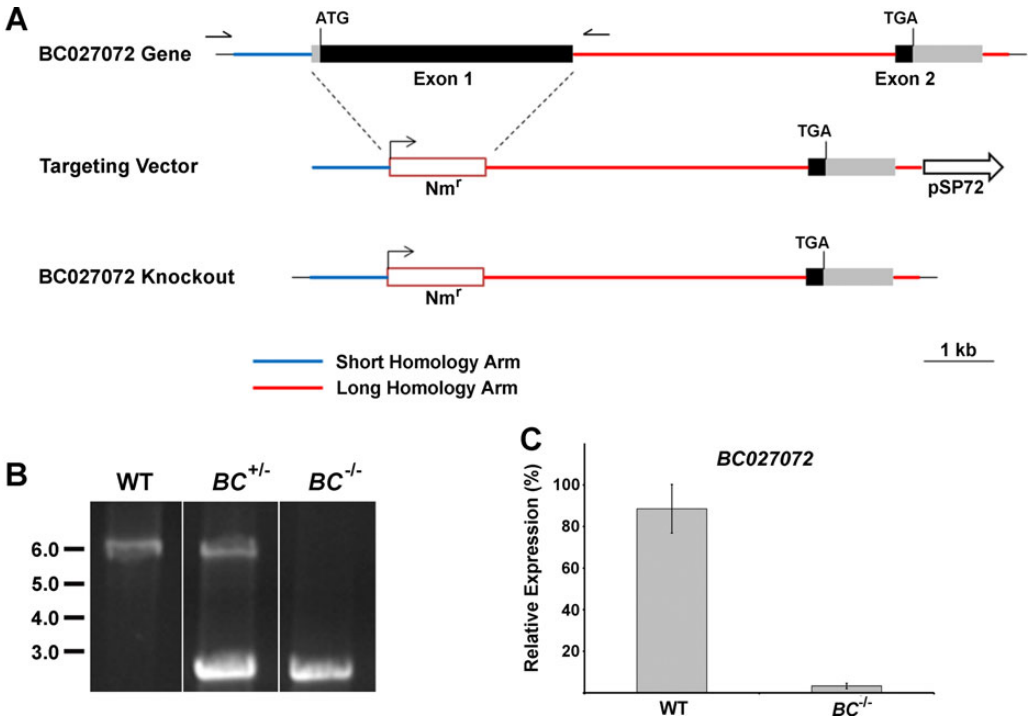

Figure 4. Targeting strategy and genotypic analysis for $BC^{-/-}$ mice. (**A**) Diagram of the knockout strategy. Blue and red regions correspond to short and long homology arms, respectively. One-sided arrows represent location of primers used for genotypic analysis. Nmr, neomycin resistance gene. (**B**) Genotypic analysis of knockout using PCR. The 6 kb band corresponds to a fragment including a WT copy of exon 1 and the 2.5 kb band represents a fragment that includes the neomycin resistance gene. (**C**) qRT-PCR was used to probe total RNA isolated from eyes of both WT and $BC^{-/-}$ mice. The 18S rRNA band was used as an internal control.

thickness similar to that of WT. Three biological replicates were performed for each genotype to provide enough data for statistical analysis. Initial analysis of differentially expressed genes confirmed our knockout with no expression of BC027072. In contrast, robust expression was present in WT mice. Approximately 200 genes were found to be at least 2-fold differentially expressed between the two genotypes. Although analysis of genes more highly expressed in WT versus knockout did not provide any obvious conclusions, genes more highly expressed in the $BC^{-/-}$ mice provided some interesting findings. The most differentially expressed genes turned out to be pro-survival genes identified in other models for retinal degeneration, namely Edn2, Fgf2 and Nudt6 (Table 2) (30,31). More interestingly, there appeared to be a significant increase in a number of pro-inflammatory

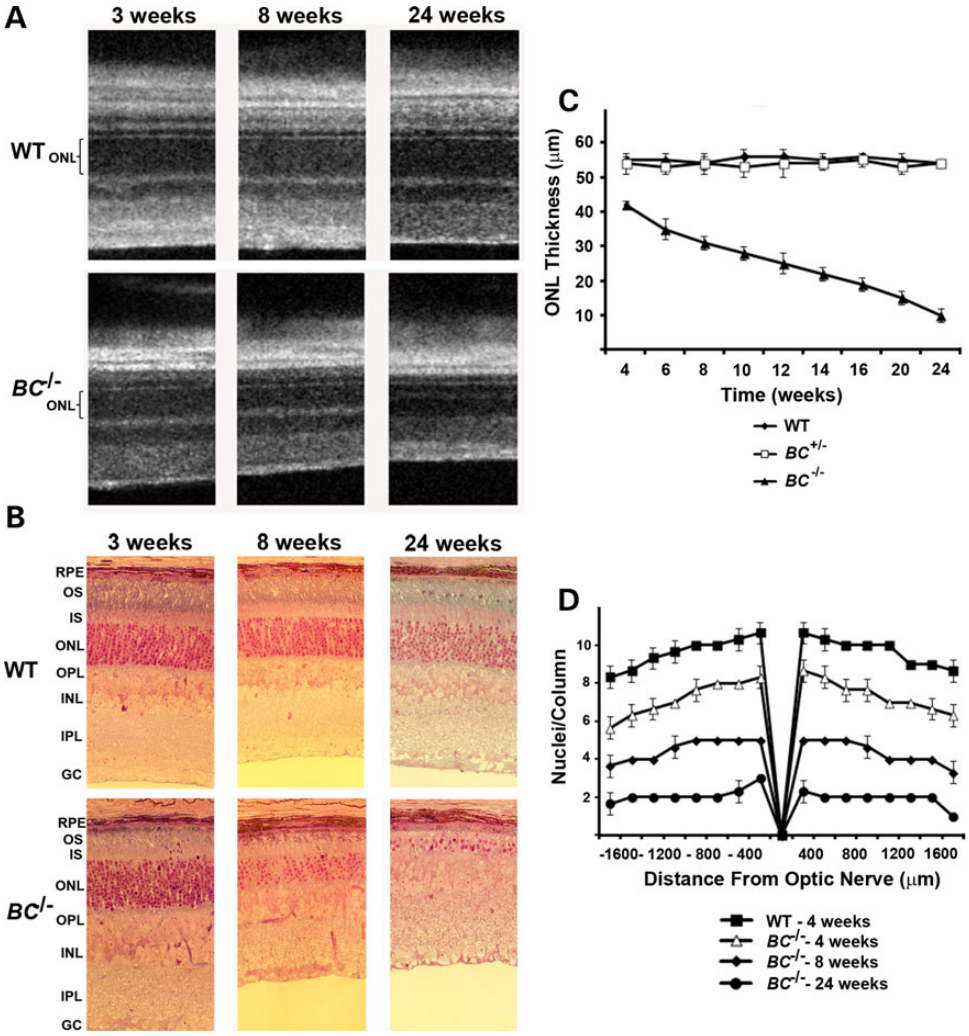

Figure 5. Analysis of mouse retinal integrity by OCT and histology. (**A**) SD-OCT imaging of WT and $BC^{-/-}$ retinas from mice at indicated ages shows age-related degeneration of the outer retina. (**B**) Light microscopic images of plastic-embedded retinas from WT and $BC^{-/-}$ mice at indicated ages demonstrate the outer retinal degeneration imaged by OCT represents a loss of photoreceptor cells as noted by the diminished ONL. (**C**) Line graph mapping of the time-dependent degeneration of ONL thickness analyzed by SD-OCT in $BC^{-/-}$ versus WT and $BC^{+/-}$ mice. (**D**) Graph representing ONL thickness from the superior to inferior retina in $BC^{-/-}$ and WT mice at indicated ages analyzed by histology of plastic-embedded eyes.

and major histocompatibility complex genes, 31 of which were 1.5-fold higher in $BC^{-/-}$ mice (Table 2). Several, including Cfi, Bcl3 and Cebpb were more than 4-fold higher in $BC^{-/-}$ mice (Table 2). Although only a small fraction of genes expressed in the eye showed a significant difference between genotypes, the increased expression of these pro-inflammatory genes suggests that this pathway could play a significant role in the rapid, progressive degeneration that we observed.

Discussion

Recently, several families with autosomal recessive RP were genetically mapped and the causative gene was identified as an uncharacterized open reading frame, *C2Orf71*, which encoded a peptide that showed no homology with any other known protein (17,18). Close inspection identified two exons, one of which accounted for >95% of the coding region. Aside from a potential lipid modification motif at the extreme N-terminus, no other information could be obtained from the primary sequence, presenting a dilemma for understanding its function. Database searches revealed the presence of this gene in the vertebrate classes of mammals, birds and fish but not in the superclass Agnatha, suggesting that this gene emerged after the divergence of jawed and jawless vertebrates (32) (Fig. 1B). Sequence comparison between human, cow, mouse and chicken shows areas of significant homology, possibly owing to the importance of these areas (Fig. 1). Initial characterizations demonstrated that the gene was likely most highly expressed in the eye, specifically the retina, and that knockdown of this gene in zebrafish resulted in an altered behavioral response to light consistent with a visual defect (17,18). Heterologous expression in mammalian cells showed that the WT protein localized to centrosomes and that mutation of either of the two lipid modification sites caused an aberrant localization to the cytosol. Additionally, if the cells were induced to produce a ciliary structure by serum deprivation, the WT protein was found to localize to this structure, suggesting a possible localization in the CC of photoreceptor cells (17). The intriguing nature of this minimally characterized protein initiated our current study.

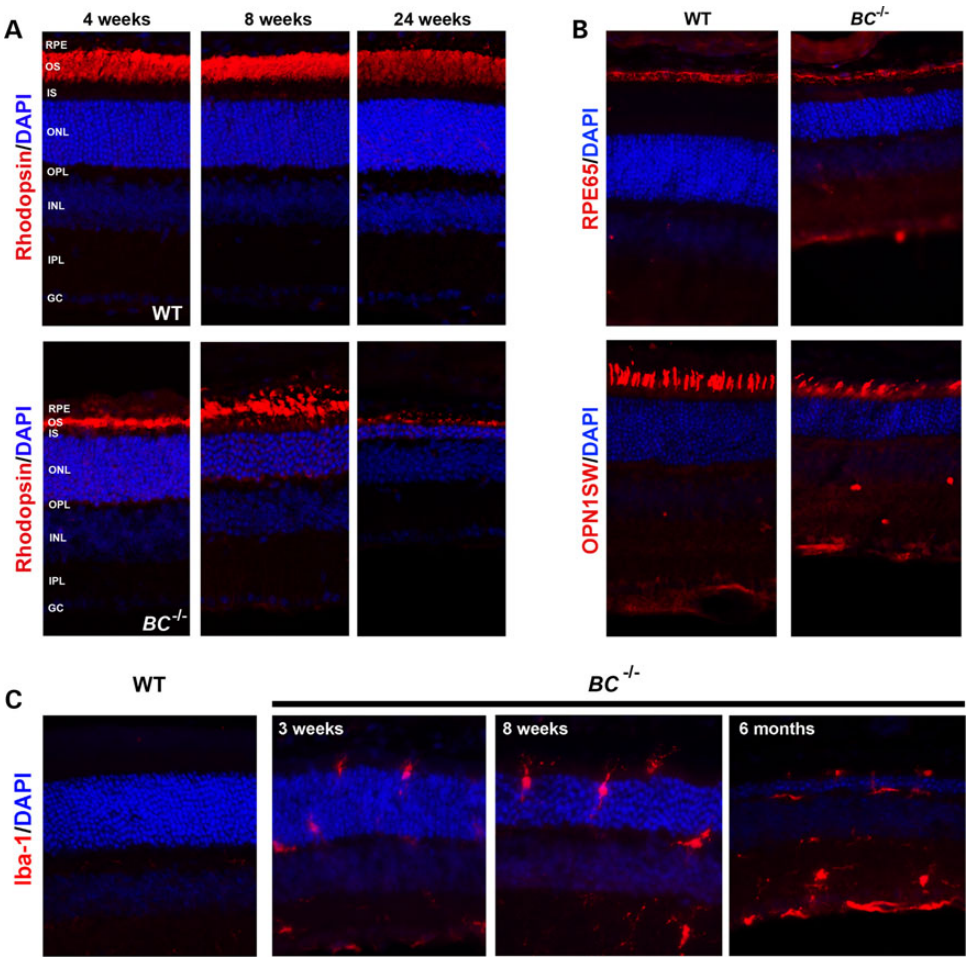

Figure 6. IHC of retinas from $BC^{-/-}$ mice. (**A**) Cryosections from 4-, 8- and 24-week-old animals were probed with anti-rhodopsin antibody for rod cells (1D4; *red*) and DAPI for nuclei (*blue*). Staining shows a highly disorganized OS region as well as rhodopsin staining in the inner nuclear layer of $BC^{-/-}$ mice. (**B**) Cryosections from 8-week-old WT and $BC^{-/-}$ mice were probed with anti-RPE65 (red), for RPE cells, or anti-OPN1SW (red), for blue cones, and DAPI for nuclei (blue). Staining is similar for RPE65 but aberrant for OPN1SW, consistent with a defect in both rods and cones. (**C**) IHC with anti-Iba-1 Ab (*red*) and DAPI (*blue*) is shown. Infiltration by activated microglia can be seen as early as 3 weeks in the $BC^{-/-}$ mice, with increasing numbers as the animal ages.

Although initial characterization of this gene provided clues to its localization and potential function, more detailed study was needed to confirm its localization in a mammalian animal model. qRT-PCR analysis demonstrated that the retina was the highest expressing tissue of those assayed. However, this expression analysis was limited to studying large portions of a tissue when the neural retina alone, a complex post-mitotic tissue, contains at least 50 different cell types. At an even finer level, photoreceptor cells are highly polarized with distinct subcellular structures (32). Development of a BC027072 pAb permitted the use of IHC which confirmed the expression of BC027072 in the retina and more specifically to the IS of photoreceptor cells, as well as the OS of cone cells. Localization of BC027072 to the IS and OS of photoreceptor cells provides a framework to generate workable hypotheses about this protein's function.

Patients who were confirmed to have mutations in *C2Orf71* displayed classic symptoms of RP with bone spicule pigmentations, night blindness, optic disc pallor, narrowing of blood vessels and progressive loss of ERG responses resulting in legal blindness. The age of onset of symptoms for individuals was always early and by the time they were 30–40 years of age each had an undetectable full field ERG (19). Additionally, these individuals also presented with a thinning of the fovea as measured by SD-OCT. This type of early-onset and rapid retinal degeneration is nearly identical to that observed in the $BC^{-/-}$ mouse. Such knockout mice showed a reduced ERG response by 4 weeks of age and nearly undetectable ERG responses by 8 weeks. Histological analysis of these mice at 3 weeks of age showed that the ONL was similar in thickness to that of WT animals but the OS exhibited severe disorganization. ONL thickness then showed a rapid and severe reduction as the mice aged and this cell layer had almost completely gone by 6 months. Recapitulation of the human pathogenesis by our $BC^{-/-}$ mouse model demonstrates that it should be an important tool in the development of any treatments for this form of RP.

The underlying causes of many degenerative pathologies are often not obvious. Accumulation of OS proteins, such as rhodopsin, has been seen in a number of ciliopathy models such as *Rp1*-deficient and $Fam161a^{GT/GT}$ or $Lca5^{GT/GT}$ gene trapped mice as well as a number of the BBSome knockout models (33–36). It is believed that mislocalization of these OS proteins is the cause of these degenerations due to defective transport of these proteins across the CC. Our IHC study of rhodopsin levels in $BC^{-/-}$ mice showed that this protein was in fact transported to the OS but

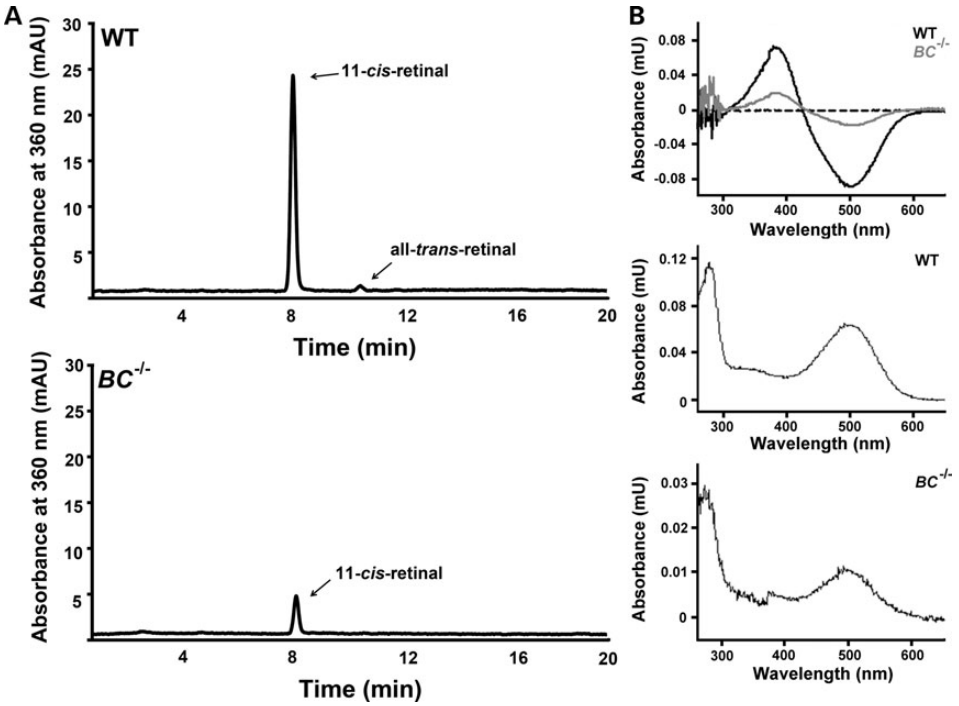

Figure 7. Retinoid and rhodopsin analysis of $BC^{-/-}$ mice. (**A**) Total retinoids were extracted from 3-week-old dark-adapted animals and analyzed by normal phase HPLC. Quantification of areas under the peak of 11-*cis*-retinal based on our standard curve determined WT and $BC^{-/-}$levels to be 277.8 ± 11 and 63.8 ± 0.9 pmol/eye, respectively. (**B**) Isolated rhodopsin was analyzed spectrophotometrically to determine the amount of bound chromophore, results showed 8.6 µg of rhodopsin/retina for WT while only 1.4 µg of rhodopsin/retina in $BC^{-/-}$. Both rhodopsin and retinoid analyses showed that $BC^{-/-}$ mice contained <20% of the WT amounts.

also that a significant amount was retained in the IS and ONL, suggesting that BC027072 could be involved in protein transport across the CC. This conclusion is consistent with the findings of Pazour *et al.* (37) in which mutant IFT88, a component of the intraflagellar transport particle, caused disorganized OS strikingly similar to those in our $BC^{-/-}$ mice. Although the degeneration in their model was not as severe as $BC^{-/-}$ in young animals, it followed a similar pattern with disorganized OS by P45 and a nearly complete absence of the photoreceptor layer by P84. More interestingly, close inspection of OS morphology in $rp1^{-/-}$ animals demonstrated a nearly identical phenocopy to our $BC^{-/-}$ model (33,38). Animals displayed highly disorganized OS regions as early as 10 days, suggesting that the OS never fully develop. Additionally, the progression of retinal degeneration occurred over a nearly identical time course as our $BC^{-/-}$ mice with an ONL thickness of approximately two nuclei by 24 weeks of age. RP1 is a microtubule-associated protein which localizes to the axoneme of the photoreceptor cell, a structure important for transport from the IS to the OS and the integrity of the OS (39). Because BC027072 localizes to a similar region of the photoreceptor cell and has an astonishingly similar phenotype when mutated, it is conceivable that both these proteins participate in the same process. EM imaging of our $BC^{-/-}$ animals revealed that the CC organization and morphology appeared to be normal, arguing against a role in the development of this structure. Instead, this finding, along with the accumulation of rhodopsin in the IS, strongly suggests a role of BC027072 in intraflagellar transport across the CC (40).

Several studies have demonstrated that microglial activation is closely tied to photoreceptor death in some forms of retinal degeneration (41–43). It was recently found that massive retinal degeneration can result in the inability of RPE cells to efficiently remove cellular material from the interphotoreceptor matrix, resulting in the infiltration of immune cells such as microglia and macrophages (44–48). EM analysis of our $BC^{-/-}$ mice showed large amounts of what appeared to be packets of photoreceptor material present in RPE cells, in stark contrast to the RPE of WT animals. Because the degeneration observed in $BC^{-/-}$ mice was similar to that found in abnormal RPE cells, we set out to determine if this retinal degeneration also leads to an infiltration of immune cells. Cryosections probed for Iba-1, an activated microglia marker, showed significant invasion of the outer retina with activated microglia cells even in our 3-week-old mutant mice. Such cells can secrete neurotoxic substances that could accelerate photoreceptor cell death (49–51). Thus it is likely that this invasion by microglia, initiated by abnormal OS development, contributes to the massive retinal degeneration observed.

Advancements in high-throughput genome sequencing paired with homozygosity mapping are revolutionizing the study of congenital diseases. The ability to quickly map a disease-causing locus with only a few individuals from a single family holds great promise for identifying causative genetic defects for hereditary diseases. Together with the analyses of the entire transcriptome of a tissue or cell line, this approach has transformed the analysis of disease states in animal models. Recently, RNASeq was used to analyze the transcriptome of the eye from animals where the transcription factor Nrl was knocked out and which recapitulates the human disease enhanced S-cone syndrome (52) and for a spontaneous cone degeneration mouse model (53). The first analysis of this transcriptome was used to show that a deficiency in the ability of the neighboring RPE to phagocytize photoreceptor OS resulted in a progressive retinal degeneration, ultimately leading to blindness. The second study showed genetic signatures of an uncompensated

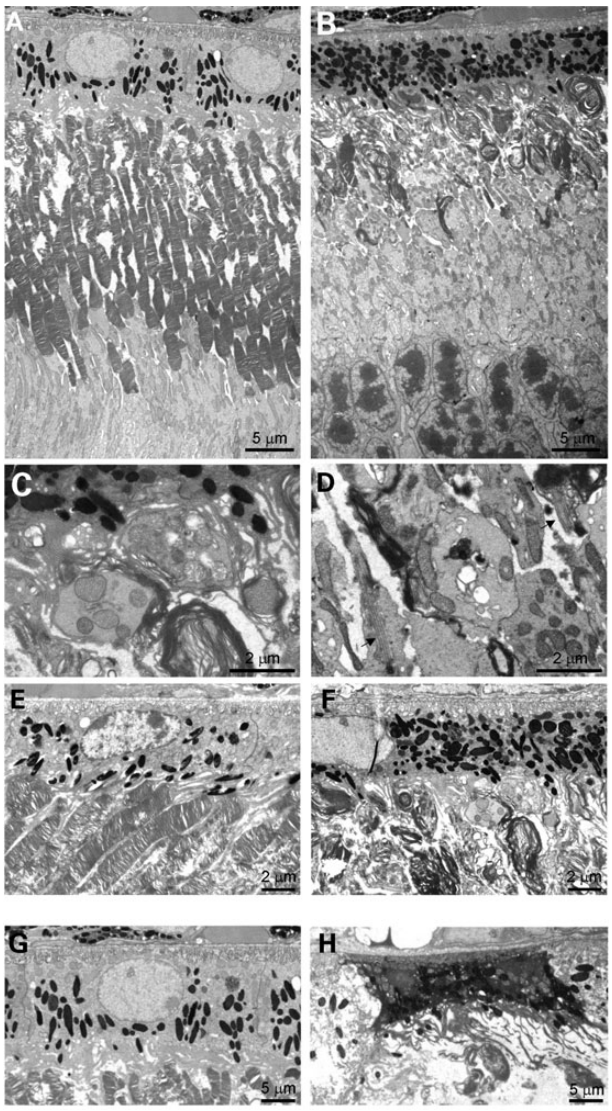

Figure 8. EM analysis of $BC^{-/-}$ mouse retinas. Eyes from 3-week-old WT (**A**) and $BC^{-/-}$ (**B**) mice were embedded in plastic and 70 μm sections were analyzed by EM. Micrographs of $BC^{-/-}$ retinal cross sections show a highly disorganized OS region which is significantly shorter than seen in WT retinas. (**C**) $BC^{-/-}$ mice exhibited packets of the IS material immediately adjacent to the RPE. (**D**) $BC^{-/-}$ photoreceptor cells had CC which were intact but lacked a connection to the OS (asterisks). $BC^{-/-}$ RPE cells (**F**) showed accumulation of massive amounts of undigested material when compared with WT (**E**) RPE cells. Necrotic RPE cells can be periodically found in 8-week-old $BC^{-/-}$ (**H**) which are dramatically different than WT RPE cells (**G**) of similar age.

preinflammatory state in these mice resulting in premature cone degeneration. We used this technology to understand the nature of the degeneration seen in our $BC^{-/-}$ mice. Animals were analyzed at three weeks of age because the photoreceptor layer is relatively intact, whereas the OS layer is already highly disorganized. Our analysis revealed that three of the most differentially expressed genes that were higher in $BC^{-/-}$ mice were the pro-survival genes *Edn2*, *Fgf2* and *Nudt6*. These genes were noted to be upregulated in a number of other retinal degenerative models and are believed to induce pro-survival pathways directed at rescuing photoreceptor cells (30,31). More interestingly, there was also a significant increase in genes associated with the pro-inflammatory response and the major histocompatibility complex. We identified 31 genes from these two classes which are upregulated at least 1.5-fold compared with WT, with three (*Cfi*, *Cebpb* and *Bcl3*) which were increased more than 4-fold. We believe that the mislocalization of a number of OS proteins, most notably rhodopsin, results in this photoreceptor dysfunction. This dysfunction ultimately includes these pro-inflammatory pathways and death of the cells, which in turn causes invasion of activated microglia, as seen by our IHC data (54,55).

Although we can speculate about this protein's function based on its localization and the type of retinal degeneration noted in $BC^{-/-}$ mice, we have yet to definitively relate it to a specific cellular process. Efforts to pull down interacting partners with our pAb have thus far been unsuccessful. Additionally, using the full-length protein as bait, we screened a yeast-two hybrid library generated from mouse retina RNA, but failed to pull out any positive interactions. Careful analysis of our EM images showed that ablation of this gene did not produce abnormal CC morphology, as had been seen in other models (8). Interestingly, we did not observe any physical connections of CCs to OS similar to those of WT animals, even at 3 weeks of age. At this early stage, the laminated structure of the retina in $BC^{-/-}$ mice is nearly intact, with a normal number of ONL nuclei, suggesting that the BC027072 protein is not required for early development and differentiation of photoreceptor cells. That said, these 3-week-old animals were almost completely unresponsive to light, as demonstrated by ERG analysis and by 8 weeks of age their ERG recordings were nearly flat. Although we have yet to demonstrate a distinct function for this protein, it does appear essential for normal photoreceptor cell maintenance and vision. Lack of even a low homology to any known proteins or even to a small domain makes this protein critical to understanding the cell biology of rod and cone photoreceptor cells.

Materials and Methods

Animals

All mice were housed in the animal facility at the School of Medicine, Case Western Reserve University under a 12-h light (~10 lux)/12-h dark cyclic environment. All animal procedures and experiments were approved by the Case Western Reserve University Animal Care Committees and conformed to recommendations of both the American Veterinary Medical Association Panel on Euthanasia and the Association of Research for Vision and Ophthalmology. C57BL/6J mice used for backcrosses or as negative controls were purchased from The Jackson Laboratory (Bar Harbor, ME). $BC^{-/-}$ were generated by inGenious Targeting Laboratories (Ronkonkoma, NY) using a standard protocol. For generation, the targeting construct was electroporated into C57BL/6N ES cells from Taconic. This genetic background was recently determined to contain the *rd8* mutation that in the homozygous state can lead to unpredictable retinal phenotypes (56). Genotyping of P_1 pups showed the presence of the *rd8* mutation. To remove this mutation, we backcrossed our heterozygous $BC^{-/+}$ three successive times with C57BL/6J animals which resulted in an *rd8* negative germline. Mice were genotyped for the neomycin cassette insert using the primers; forward: 5′-GTCAAG AAACC CAGCCTGAAAGG-3′; reverse: 5′-CCAGAGGCCACTTGTGTAGC-3′. Either age-matched negative littermates or C57BL/6J mice were used as negative controls.

qRT-PCR

Total RNA was isolated from mouse brain, heart, lung, spleen, testes, kidney, stomach, large intestine, small intestine, liver,

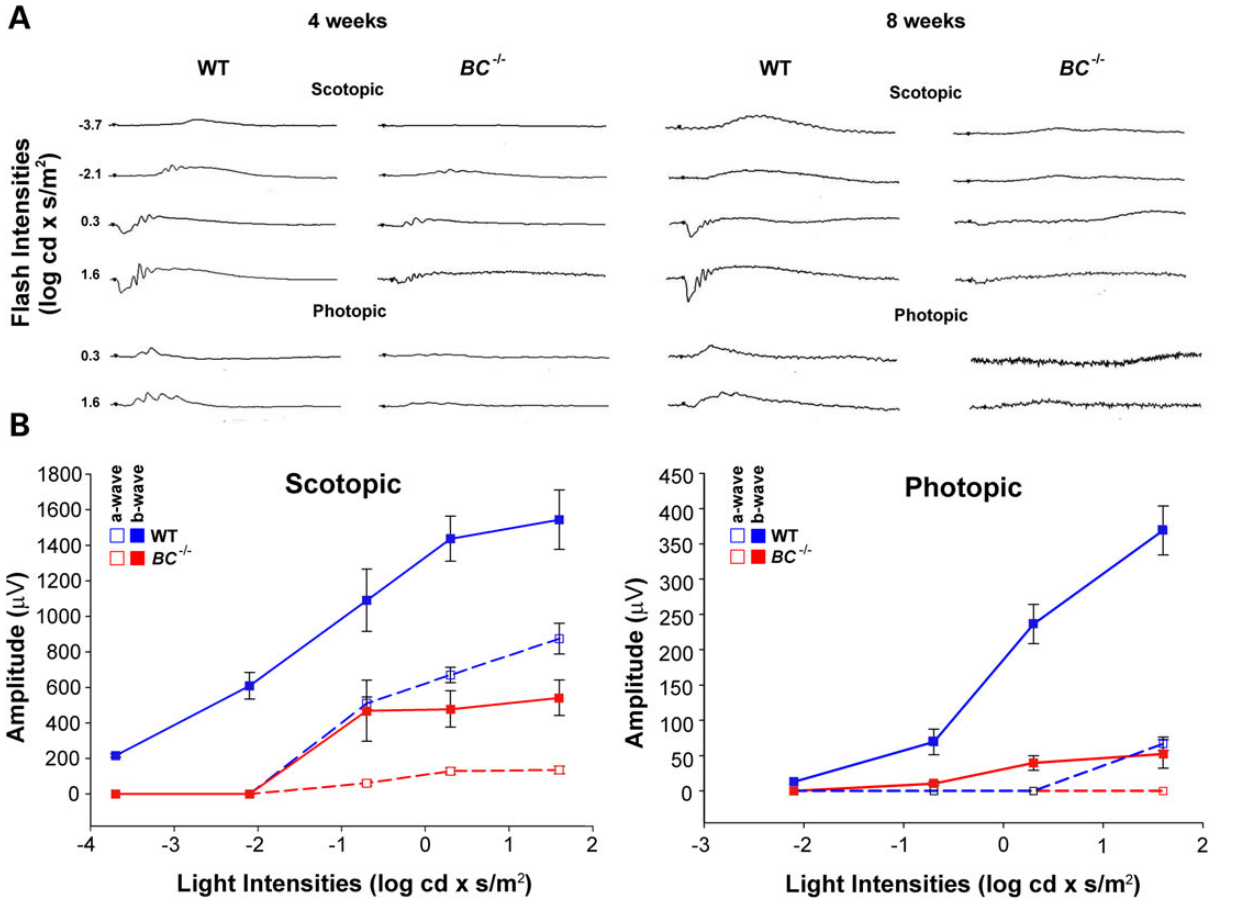

Figure 9. ERG analysis of $BC^{-/-}$ mice. (**A**) Representative full-field scotopic and photopic ERG responses of anesthetized WT and $BC^{-/-}$ mice at 4 and 8 weeks of age show reduced scotopic and photopic responses in $BC^{-/-}$when compared with WT animals. Whereas WT mice showed a robust response to increasing intensities of light, $BC^{-/-}$ mice evidenced a nearly flat response by 8 weeks of age. (**B**) Amplitudes of both rod photoreceptor cell-evoked scotopic (left) a- and b-waves and cone photoreceptor cell-dependent photopic (right) a- and b-waves were reduced in 8-week-old $BC^{-/-}$ mice ($n > 4$).

Table 2. Differential gene expression between WT and $BC^{-/-}$ mice

Higher in WT mice	WT	BC027072 KO	Fold difference
BC027072	53.94	0.06	844.4
Glb1l3	1.45	0.15	9.7
Serpine3	24.04	2.74	8.8
Ankrd2	2.19	0.56	3.9
1700027L20Rik	4.44	1.22	3.6
Hba-a1,Hba-a2	149.81	47.18	3.2
Rasl11a	5.85	1.89	3.1
Wfikkn2	14.12	4.65	3.0
Higher in $BC^{-/-}$ mice			
Edn2	0.66	36.19	55.0
Fgf2	6.91	42.09	6.1
Cfi	0.27	1.52	5.7
Nudt6	4.24	20.59	4.9
Lrrc2	2.81	13.18	4.7
Cepbp	4.30	18.88	4.4
Bcl3	1.73	7.40	4.3
Fhad1	0.64	2.55	4.0
H2-Q7,H2-Q9	0.66	2.54	3.9

Values represented as FPKM reads.

eye and bladder in triplicate with the Qiagen RNeasy kit. cDNAs were generated with the High Capacity RNA-to-cDNA kit from Applied Biosystems (Grand Island, NY). Real-time PCR amplification was performed with the Taqman Gene Expression Assay kit (Invitrogen; Grand Island, NY). BC027072 and 18S rRNA control primer/probe sets employed for the Taqman assay were purchased from Invitrogen (BC027072: #4351372; 18S: 4453320). Analyses were performed in the comparative Ct mode with an Applied Biosystems StepOnePlus Real-Time PCR machine (Grand Island, NY).

RNASeq analyses

RNASeq library construction, sample runs and data analyses were performed as previously described (52). Each reported measurement represents an average of at least three biological replicates.

BC027072 antibody generation and immunoblot analyses

For antibody generation, full-length BC027072 was first cloned from a C57BL/6J mouse eye cDNA library, then subcloned into the pIEx vector (EMD Millipore, Billerica, MA) and verified by Sanger sequencing. Recombinant baculovirus was produced

with the flashBac Expression System (Oxford Expression Technologies, Oxford, UK) according to manufacturer's directions. P2 virus was employed to infect Sf9 cells in a suspension culture and grown for an additional 3 days at 28°C. Cells were harvested and stored at −80°C until use. For protein purification, cells were thawed on ice and resuspended in 50 mM Tris–HCl, pH 8.0, 300 mM NaCl. The cell suspension was sonicated to lyse the cells and spun at 20 000*g* for 30 min at 4°C. Because the protein partitioned with membrane fraction, the pellet was resuspended in 50 mM Tris–HCl, pH 8.0, 300 mM NaCl, 30 mM Fos-Choline 12, 5 mM imidazole and incubated at 4°C for 2 h with agitation. To clear insoluble material, the lysate was spun at 150 000*g* for 1 h at 4°C. Forty milliliters of cleared lysate was run over a commercial 5 ml IMAC Column (Bio-Rad, Hercules, CA) pre-equilibrated with 10 column volumes (CVs) of 50 mM Tris–HCl, pH 8.0, 300 mM NaCl, 3 mM Fos-Choline 12, 5 mM imidazole. The column was washed with 20 CVs of 50 mM Tris–HCl, pH 8.0, 300 mM NaCl, 3 mM Fos-Choline 12, 10 mM imidazole and then eluted with buffer containing 250 mM imidazole. Protein was concentrated to 1 mg/ml with a 100 kDa cutoff Amicon Ultra Centrifugal Concentrator (EMD Millipore, Billerica, MA) and submitted to Cocalico Biologicals (Reamstown, PA) for pAb production in rabbits. Anti BC027072 serum was used directly to screen against recombinant protein and native eye tissue to determine the success of immunizations. Polyclonal antibody was purified from serum with thiophilic adsorbent resin according to manufacturer's instructions (Thermo Scientific, Waltham, MA). Protein used for immunoblot analyses was isolated from freshly dissected tissues by manual homogenization in 1× radioimmunoprecipitation assay buffer (RIPA; 20 mM Tris–HCl, pH 7.5, 150 mM NaCl, 1 mM ethylenediaminetetraacetic acid, 1 mM ethylene glycol tetraacetic acid, 1% NP-40, 1% sodium deoxycholate, 1× protease inhibitors). The lysate was incubated on ice for 30 min and subsequently centrifuged at 15 000*g* for 20 min at 4°C. Immunoblot analysis was conducted according to established protocols (57) with purified pAb that was concentrated to 2 mg/ml in a 100 kDa cutoff Amicon Ultra Centrifugal Concentrator and used at a concentration of 1:1000. Peroxidase-labeled secondary antibodies (Jackson ImmunoResearch Laboratories, West Grove, PA) were employed directly from purchased stock at a 1:5000 dilution and visualized with a Supersignal West Pico Chemiluminescent Substrate kit (Thermo Scientific).

IHC

For embedding, eyes of WT or $BC^{-/-}$ mice were removed and placed in 4% paraformaldehyde in phosphate-buffered saline (PBS, 137 mM NaCl, 2.7 mM KCl, 10 mM Na_2HPO_4, 1.8 mM KH_2PO_4) (58). Both cornea and lens were dissected from the eyeballs and eye cups were placed in fresh paraformaldehyde and incubated at 4°C overnight with gentle agitation. Eye cups then were dehydrated in 15% sucrose in PBS for 8 h at 4°C and overnight in 30% sucrose in PBS with gentle agitation. Dehydrated eye cups were immersed in a 1:1 solution of optimum cutting temperature compound (O.C.T.) (Tissue Tek, Torrance, CA) and 30% sucrose and incubated overnight at 4°C with gentle agitation. Finally, eye cups were placed in vinyl cryomolds (Tissue Tek) along with 1:1 O.C.T.: 30% sucrose and rapidly frozen in a bath of 2-methylbutane floating in liquid nitrogen. Cryoblocks were stored at −80°C until sectioning. Cryosections (12 µm) were cut with a Tissue Tek II Cryostat (Torrance, CA) and placed on Superfrost Plus microscope slides (Fisher Scientific, Pittsburgh, PA). Sections were dried and stored at −80°C until use. For IHC, sections were permeabilized and blocked in 0.2% Triton X-100/PBS with 5% goat serum for 30 min at room temperature (58). Sections were washed in PBS and then incubated overnight at 4°C with the following indicated primary antibodies: 1D4 mAb (1:10 000), biotinylated-PNA (1:1000), BC027072 pAb (1:50), RPE65 (1:100) or OPN1SW (1:200) from (Millipore, Billerica, MA); or Iba-1 (1:400) from (Wako Chemicals USA, Richmond, VA), all in 0.2% Triton X-100/PBS. Sections then were washed with PBS and incubated with appropriate fluorescently conjugated secondary antibodies (Jackson ImmunoResearch Laboratories) for 1 h at room temperature. Afterwards sections were washed in PBS and incubated with 4',6-diamidino-2-phenylindole (DAPI) stain (Life Technologies, Carlsbad, CA) for 30 min at room temperature. Sections were washed and mounted with a coverslip using Fluoromount G (EMS, Hatfield, PA). Imaging was accomplished with a Leica TCS SP5 II Confocal Microscope (Wetzlar, Germany) (59).

SD-OCT

SD-OCT (Envisu™ C-Class SDOIS; Bioptigen, Research Triangle Park, NC) was employed for *in vivo* imaging of mouse retinas (29). Mice were anesthetized by intraperitoneal injection of a mixture (20 µl/g of body weight) containing ketamine (6 mg/ml) and xylazine (0.44 mg/ml) in 10 mM sodium phosphate, pH 7.2 and 100 mM NaCl. Pupils were dilated with a mixture of 0.5% tropicamide and 0.5% phenylephrine hydrochloride (Midorin-P, Santen Pharmaceutical Co., Ltd.). Quantification of ONL thickness was performed with calipers in the Bioptigen InVivoVue software package and at least five images were used to average the data.

Electron microscopy

Mice were euthanized by cervical dislocation and eyes were removed and placed in 4% paraformaldehyde/dimethyl sulfoxide and incubated at room temperature for 2 h. Eponate embedding was performed by established protocols (60). Thick sections (1 µm) were used for light microscopic analysis and ultra-thin sections (70 nm) were adhered to carbon-coated EM grids and negatively stained with uranyl acetate for transmission EM. Imaging was performed with a Zeiss CEM902 EM (Oberkochen, Germany).

HPLC analysis of retinoids

All experimental procedures related to extraction, derivatization and separation of retinoids from dissected mouse eyes were carried out under dim red light as described previously (61). Retinoids were separated by normal phase HPLC (Ultrasphere-Si, 4.6 µm, 250 mm; Beckman, Fullerton, CA) with 10% ethyl acetate and 90% hexane at a flow rate of 1.4 ml/min with detection at 325 nm by using an HP1100 HPLC with a diode array detector and HP Chemstation A.03.03 software.

Rhodopsin analysis

Retinas from WT and $BC^{-/-}$ mice ($n = 5$) were dissected away from the RPE/choroid and manually homogenized in 500 µl of 10 mM Bis–Tris propane, pH 7.5, 100 mM NaCl. Cells were solubilized by addition of 20 mM dodecyl maltoside and incubated on ice for 45 min. Insoluble material was removed by centrifugation at 185 000*g* at 4°C. The cleared lysate (500 µl) was split into 200 and 300 µl aliquots. A spectrum of the 200 µl sample was immediately measured in a spectrophotometer, the sample was then bleached and the spectrum was measured again to obtain a difference spectrum. The 300 µl sample was used to purify rhodopsin by affinity chromatography on customized 1D4 antibody-

conjugated CNBr resin (28). Here, the sample was eluted by addition of the 1D4 peptide (TETSQVAPA) and its spectrum was subsequently measured with the spectrophotometer (Cary 50; Varian, Palo Alto, CA). Differences between the WT and $BC^{-/-}$ spectra were determined at 500 nm.

ERG analyses

Prior to recording, mice were dark-adapted for 48 h. Then mice under safety light were anesthetized by intraperitoneal injection of 20 µl/g body weight of 6 mg/ml ketamine and 0.44 mg/ml xylazine diluted with 10 mM sodium phosphate, pH 7.2, containing 100 mM NaCl (62). Pupils were dilated with 1% tropicamide. A contact lens electrode was placed on the eye, and a reference electrode and ground electrode were placed in the ear and on the tail, respectively (62). ERGs were recorded with the universal testing and electrophysiological system UTAS E-3000 (LKC Technologies, Inc., Gaithersburg, MD).

Acknowledgements

We thank Dr Leslie T. Webster Jr and members of Palczewski's laboratory for helpful comments on this manuscript and Dr Yoshikazu Imanishi and Debarshi Mustafi (all from CWRU) for support and advice during this study.

Conflict of Interest statement. None declared.

Funding

This work was supported by funding from the National Institutes of Health, EY009339 (K.P.) and EY021126 (K.P., John H. Hord Professor of Pharmacology).

References

1. Palczewski, K. (2012) Chemistry and biology of vision. *J. Biol. Chem.*, **287**, 1612–1619.
2. Hildebrand, G.D. and Fielder, A.R. (2011) Anatomy and physiology of the retina. In Reynolds, J.D. and Olitsky, S.E. (eds), *Pediatric Retina*. Springer, Berlin, Germany, pp. 39–65.
3. Ridge, K.D., Abdulaev, N.G., Sousa, M. and Palczewski, K. (2003) Phototransduction: crystal clear. *Trends Biochem. Sci.*, **28**, 479–487.
4. Sahel, J., Bonnel, S., Mrejen, S. and Paques, M. (2010) Retinitis pigmentosa and other dystrophies. In Coscas, G., CunhaVaz, J., Loewenstein, A. and Soubrane, G. (eds), *Macular Edema: A Practical Approach*. Karger, Postfach, Basel, Switzerland, Vol. 47, pp. 160–167.
5. Anasagasti, A., Irigoyen, C., Barandika, O., de Munain, A.L. and Ruiz-Ederra, J. (2012) Current mutation discovery approaches in retinitis pigmentosa. *Vision Res.*, **75**, 117–129.
6. Daiger, S.P., Sullivan, L.S. and Bowne, S.J. (2013) Genes and mutations causing retinitis pigmentosa. *Clin. Genet.*, **84**, 132–141.
7. Ferrari, S., Di Iorio, E., Barbaro, V., Ponzin, D., Sorrentino, F.S. and Parmeggiani, F. (2011) Retinitis pigmentosa: genes and disease mechanisms. *Curr. Genomics*, **12**, 238–249.
8. Karlstetter, M., Sorusch, N., Caramoy, A., Dannhausen, K., Aslanidis, A., Fauser, S., Boesl, M.R., Nagel-Wolfrum, K., Tamm, E.R., Jägle, H. *et al.* (2014) Disruption of the retinitis pigmentosa 28 gene Fam161a in mice affects photoreceptor ciliary structure and leads to progressive retinal degeneration. *Hum. Mol. Genet.*, **23**, 5197–5210.
9. Estrada-Cuzcano, A., Neveling, K., Kohl, S., Banin, E., Rotenstreich, Y., Sharon, D., Falik-Zaccai, T.C., Hipp, S., Roepman, R., Wissinger, B. *et al.* (2012) Mutations in C8orf37, encoding a ciliary protein, are associated with autosomal-recessive retinal dystrophies with early macular involvement. *Am. J. Hum. Genet.*, **90**, 102–109.
10. Zach, F., Grassmann, F., Langmann, T., Sorusch, N., Wolfrum, U. and Stohr, H. (2012) The retinitis pigmentosa 28 protein FAM161A is a novel ciliary protein involved in intermolecular protein interaction and microtubule association. *Hum. Mol. Genet.*, **21**, 4573–4586.
11. Bocquet, B., Marzouka, N.A., Hebrard, M., Manes, G., Senechal, A., Meunier, I. and Hamel, C.P. (2013) Homozygosity mapping in autosomal recessive retinitis pigmentosa families detects novel mutations. *Mol. Vis.*, **19**, 2487–2500.
12. Coppieters, F., Van Schil, K., Bauwens, M., Verdin, H., De Jaegher, A., Syx, D., Sante, T., Lefever, S., Abdelmoula, N.B., Depasse, F. *et al.* (2014) Identity-by-descent-guided mutation analysis and exome sequencing in consanguineous families reveals unusual clinical and molecular findings in retinal dystrophy. *Genet. Med.*, **16**, 671–680.
13. Zobor, D., Balousha, G., Baumann, B. and Wissinger, B. (2014) Homozygosity mapping reveals new nonsense mutation in the FAM161A gene causing autosomal recessive retinitis pigmentosa in a Palestinian family. *Mol. Vis.*, **20**, 178–182.
14. Eisenberger, T., Slim, R., Mansour, A., Nauck, M., Nurnberg, G., Nurnberg, P., Decker, C., Dafinger, C., Ebermann, I., Bergmann, C. *et al.* (2012) Targeted next-generation sequencing identifies a homozygous nonsense mutation in ABHD12, the gene underlying PHARC, in a family clinically diagnosed with Usher syndrome type 3. *Orphanet J. Rare Dis.*, **7**, 6.
15. Littink, K.W., den Hollander, A.I., Cremers, F.P.M. and Collin, R.W.J. (2012). The power of homozygosity mapping: discovery of new genetic defects in patients with retinal dystrophy. In LaVail, M.M., Ash, J.D., Anderson, R.E., Hollyfield, J.G. and Grimm, C. (eds). *Retinal Degenerative Diseases*. Springer, Berlin, Vol. 723, pp. 345–351.
16. Alkuraya, F.S. (2010) Homozygosity mapping: one more tool in the clinical geneticist's toolbox. *Genet. Med.*, **12**, 236–239.
17. Nishimura, D.Y., Baye, L.M., Perveen, R., Searby, C.C., Avila-Fernandez, A., Pereiro, I., Ayuso, C., Valverde, D., Bishop, P.N., Manson, F.D.C. *et al.* (2010) Discovery and functional analysis of a retinitis pigmentosa gene, C2ORF71. *Am. J. Hum. Genet.*, **86**, 686–695.
18. Collin, R.W.J., Safieh, C., Littink, K.W., Shalev, S.A., Garzozi, H.J., Rizel, L., Abbasi, A.H., Cremers, F.P.M., den Hollander, A.I., Klevering, B.J. *et al.* (2010) Mutations in C2ORF71 cause autosomal-recessive retinitis pigmentosa. *Am. J. Hum. Genet.*, **86**, 783–788.
19. Audo, I., Lancelot, M.E., Mohand-Said, S., Antonio, A., Germain, A., Sahel, J.A., Bhattacharya, S.S. and Zeitz, C. (2011) Novel C2orf71 mutations account for similar to 1% of cases in a large French arRP Cohort. *Hum. Mutat.*, **32**, E2091–E2103.
20. Hebrard, M., Manes, G., Bocquet, B., Meunier, I., Coustes-Chazalette, D., Herald, E., Senechal, A., Bolland-Auge, A., Zelenika, D. and Hamel, C.P. (2011) Combining gene mapping and phenotype assessment for fast mutation finding in non-consanguineous autosomal recessive retinitis pigmentosa families. *Eur. J. Hum. Genet.*, **19**, 1256–1263.
21. Khateb, S., Zelinger, L., Mizrahi-Meissonnier, L., Ayuso, C., Koenekoop, R.K., Laxer, U., Gross, M., Banin, E. and Sharon, D. (2014) A homozygous nonsense CEP250 mutation combined with a heterozygous nonsense C2orf71 mutation is associated with atypical Usher syndrome. *J. Med. Genet.*, **51**, 460–469.

22. Sergouniotis, P.I., Li, Z., Mackay, D.S., Wright, G.A., Borman, A. D., Devery, S.R., Moore, A.T. and Webster, A.R. (2011) A survey of DNA variation of C2ORF71 in probands with progressive autosomal recessive retinal degeneration and controls. *Invest. Ophthalmol. Vis. Sci.*, **52**, 1880–1886.
23. Rocque, W.J., McWherter, C.A., Wood, D.C. and Gordon, J.I. (1993) A comparative-analysis of the kinetic mechanism and peptide substrate-specificity of human and *Saccharomyces cerevisiae* myristoyl-coa:protein N-myristoyltransferase. *J. Biol. Chem.*, **268**, 9964–9971.
24. Aicart-Ramos, C., Valero, R.A. and Rodriguez-Crespo, I. (2011) Protein palmitoylation and subcellular trafficking. *Biochim. Biophys. Acta*, **1808**, 2981–2994.
25. Soumillon, M., Necsulea, A., Weier, M., Brawand, D., Zhang, X.L., Gu, H.C., Barthes, P., Kokkinaki, M., Nef, S., Gnirke, A. *et al.* (2013) Cellular source and mechanisms of high transcriptome complexity in the mammalian testis. *Cell Rep.*, **3**, 2179–2190.
26. Tsybovsky, Y., Molday, R.S. and Palczewski, K. (2010) The ATP-binding cassette transporter ABCA4: structural and functional properties and role in retinal disease. *Adv. Exp. Med. Biol.*, **703**, 105–125.
27. Soucy, E., Wang, Y., Nirenberg, S., Nathans, J. and Meister, M. (1998) A novel signaling pathway from rod photoreceptors to ganglion cells in mammalian retina. *Neuron*, **21**, 481–493.
28. Jastrzebska, B., Golczak, M., Fotiadis, D., Engel, A. and Palczewski, K. (2009) Isolation and functional characterization of a stable complex between photoactivated rhodopsin and the G protein, transducin. *FASEB J.*, **23**, 371–381.
29. Maeda, A., Golczak, M., Chen, Y., Okano, K., Kohno, H., Shiose, S., Ishikawa, K., Harte, W., Palczewska, G., Maeda, T. *et al.* (2012) Primary amines protect against retinal degeneration in mouse models of retinopathies. *Nat. Chem. Biol.*, **8**, 170–178.
30. Bramall, A.N., Szego, M.J., Pacione, L.R., Chang, I., Diez, E., D'Orleans-Juste, P., Stewart, D.J., Hauswirth, W.W., Yanagisawa, M. and McInnes, R.R. (2013) Endothelin-2-mediated protection of mutant photoreceptors in inherited photoreceptor degeneration. *PLoS One*, **8**, 14.
31. Samardzija, M., Wariwoda, H., Imsand, C., Huber, P., Heynen, S.R., Gubler, A. and Grimm, C. (2012) Activation of survival pathways in the degenerating retina of rd10 mice. *Exp. Eye Res.*, **99**, 17–26.
32. Lamb, T.D. (2013) Evolution of phototransduction, vertebrate photoreceptors and retina. *Prog. Retin. Eye Res.*, **36**, 52–119.
33. Liu, Q., Lyubarsky, A., Skalet, J.H., Pugh, E.N. and Pierce, E.A. (2003) RP1 is required for the correct stacking of outer segment discs. *Invest. Ophthalmol. Vis. Sci.*, **44**, 4171–4183.
34. Boldt, K., Mans, D.A., Won, J., van Reeuwijk, J., Vogt, A., Kinkl, N., Letteboer, S.J.F., Hicks, W.L., Hurd, R.E., Naggert, J.K. *et al.* (2011) Disruption of intraflagellar protein transport in photoreceptor cilia causes Leber congenital amaurosis in humans and mice. *J. Clin. Invest.*, **121**, 2169–2180.
35. Abd-El-Barr, M.M., Sykoudis, K., Andrabi, S., Eichers, E.R., Pennesi, M.E., Tan, P.L., Wilson, J.H., Katsanis, N., Lupski, J.R. and Wu, S.M. (2007) Impaired photoreceptor protein transport and synaptic transmission in a mouse model of Bardet–Biedl syndrome. *Vision Res.*, **47**, 3394–3407.
36. Nishimura, D.Y., Fath, M., Mullins, R.F., Searby, C., Andrews, M., Davis, R., Andorf, J.L., Mykytyn, K., Swiderski, R.E., Yang, B.L. *et al.* (2004) Bbs2-null mice have neurosensory deficits, a defect in social dominance, and retinopathy associated with mislocalization of rhodopsin. *Proc. Natl. Acad. Sci. USA*, **101**, 16588–16593.
37. Pazour, G.J., Baker, S.A., Deane, J.A., Cole, D.G., Dickert, B.L., Rosenbaum, J.L., Witman, G.B. and Besharse, J.C. (2002) The intraflagellar transport protein, IFT88, is essential for vertebrate photoreceptor assembly and maintenance. *J. Cell Biol.*, **157**, 103–113.
38. Gao, J.G., Cheon, K., Nusinowitz, S., Liu, Q., Bei, D., Atkins, K., Azimi, A., Daiger, S.P., Farber, D.B., Heckenlively, J.R. *et al.* (2002) Progressive photoreceptor degeneration, outer segment dysplasia, and rhodopsin mislocalization in mice with targeted disruption of the retinitis pigmentosa-1 (Rp1) gene. *Proc. Natl. Acad. Sci. USA*, **99**, 5698–5703.
39. Liu, Q., Zuo, J. and Pierce, E.A. (2004) The retinitis pigmentosa 1 protein is a photoreceptor microtubule-associated protein. *J. Neurosci.*, **24**, 6427–6436.
40. Insinna, C. and Besharse, J.C. (2008) Intraflagellar transport and the sensory outer segment of vertebrate photoreceptors. *Dev. Dyn.*, **237**, 1982–1992.
41. Reme, C.E., Grimm, C., Hafezi, F., Wenzel, A. and Williams, T.P. (2000) Apoptosis in the retina: the silent death of vision. *News Physiol. Sci.*, **15**, 120–125.
42. Wright, A.F., Chakarova, C.F., El-Aziz, M.M.A. and Bhattacharya, S.S. (2010) Photoreceptor degeneration: genetic and mechanistic dissection of a complex trait. *Nat. Rev. Genet.*, **11**, 273–284.
43. Stone, J., Maslim, J., Valter-Kocsi, K., Mervin, K., Bowers, F., Chu, Y., Barnett, N., Provis, J., Lewis, G., Fisher, S.K. *et al.* (1999) Mechanisms of photoreceptor death and survival in mammalian retina. *Prog. Retin. Eye Res.*, **18**, 689–735.
44. Kohno, H., Chen, Y., Kevany, B.M., Pearlman, E., Miyagi, M., Maeda, T., Palczewski, K. and Maeda, A. (2013) Photoreceptor proteins initiate microglial activation via toll-like receptor 4 in retinal degeneration mediated by all-trans-retinal. *J. Biol. Chem.*, **288**, 15326–15341.
45. Roque, R.S., Imperial, C.J. and Caldwell, R.B. (1996) Microglial cells invade the outer retina as photoreceptors degenerate in Royal College of Surgeons rats. *Invest. Ophthalmol. Vis. Sci.*, **37**, 196–203.
46. Noailles, A., Fernandez-Sanchez, L., Lax, P. and Cuenca, N. (2014) Microglia activation in a model of retinal degeneration and TUDCA neuroprotective effects. *J. Neuroinflammation*, **11**, 186.
47. Levine, E.S., Zam, A., Zhang, P.F., Pechko, A., Wang, X.L., Fitz-Gerald, P., Pugh, E.N., Zawadzki, R.J. and Burns, M.E. (2014) Rapid light-induced activation of retinal microglia in mice lacking Arrestin-1. *Vision Res.*, **102**, 71–79.
48. Peng, B., Xiao, J., Wang, K., So, K.F., Tipoe, G.L. and Lin, B. (2014) Suppression of microglial activation is neuroprotective in a mouse model of human retinitis pigmentosa. *J. Neurosci.*, **34**, 8139–8150.
49. Karlstetter, M., Ebert, S. and Langmann, T. (2010) Microglia in the healthy and degenerating retina: insights from novel mouse models. *Immunobiology*, **215**, 685–691.
50. Roque, R.S., Rosales, A.A., Jingjing, L., Agarwal, N. and Al-Ubaidi, M.R. (1999) Retina-derived microglial cells induce photoreceptor cell death in vitro. *Brain Res.*, **836**, 110–119.
51. Ma, W.X., Zhao, L., Fontainhas, A.M., Fariss, R.N. and Wong, W.T. (2009) Microglia in the mouse retina alter the structure and function of retinal pigmented epithelial cells: a potential cellular interaction relevant to AMD. *PLoS One*, **4**, 12.
52. Mustafi, D., Kevany, B.M., Genoud, C., Okano, K., Cideciyan, A.V., Sumaroka, A., Roman, A.J., Jacobson, S.G., Engel, A., Adams, M.D. *et al.* (2011) Defective photoreceptor phagocytosis in a mouse model of enhanced S-cone syndrome causes progressive retinal degeneration. *FASEB J.*, **25**, 3157–3176.

53. Mustafi, D., Maeda, T., Kohno, H., Nadeau, J.H. and Palczewski, K. (2012) Inflammatory priming predisposes mice to age-related retinal degeneration. *J. Clin. Invest.*, **122**, 2989–3001.
54. Karlstetter, M., Walczak, Y., Weigelt, K., Ebert, S., Van den Brulle, J., Schwer, H., Fuchshofer, R. and Langmann, T. (2010) The novel activated microglia/macrophage WAP Domain protein, AMWAP, acts as a counter-regulator of proinflammatory response. *J. Immunol.*, **185**, 3379–3390.
55. Parmeggiani, F., Sorrentino, F.S., Romano, M.R., Costagliola, C., Semeraro, F., Incorvaia, C., D'Angelo, S., Perri, P., De Nadai, K., Roversi, E.B. *et al.* (2013) Mechanism of inflammation in age-related macular degeneration: an up-to-date on genetic landmarks. *Mediat. Inflamm.*, **2013**, 1–13.
56. Mattapallil, M.J., Wawrousek, E.F., Chan, C.C., Zhao, H., Roychoudhury, J., Ferguson, T.A. and Caspi, R.R. (2012) The Rd8 mutation of the Crb1 gene is present in vendor lines of C57BL/6N mice and embryonic stem cells, and confounds ocular induced mutant phenotypes. *Invest. Ophthalmol. Vis. Sci.*, **53**, 2921–2927.
57. Kevany, B.M., Tsybovsky, Y., Campuzano, I.D.G., Schnier, P. D., Engel, A. and Palczewski, K. (2013) Structural and functional analysis of the native peripherin–ROM1 complex isolated from photoreceptor cells. *J. Biol. Chem.*, **288**, 36272–36284.
58. Amengual, J., Zhang, N., Kemerer, M., Maeda, T., Palczewski, K. and von Lintig, J. (2014) STRA6 is critical for cellular vitamin A uptake and homeostasis. *Hum. Mol. Genet.*, **23**, 5402–5417.
59. Zhang, N., Kolesnikov, A.V., Jastrzebska, B., Mustafi, D., Sawada, O., Maeda, T., Genoud, C., Engel, A., Kefalov, V.J. and Palczewski, K. (2013) Autosomal recessive retinitis pigmentosa E150 K opsin mice exhibit photoreceptor disorganization. *J. Clin. Invest.*, **123**, 121–137.
60. Imanishi, Y., Sun, W.Y., Maeda, T., Maeda, A. and Palczewski, K. (2008) Retinyl ester homeostasis in the adipose differentiation-related protein-deficient retina. *J. Biol. Chem.*, **283**, 25091–25102.
61. Golczak, M., Bereta, G., Maeda, A. and Palczewski, K. (2010) Molecular biology and analytical chemistry methods used to probe the retinoid cycle. In Sun, H. and Travis, G.H. (eds), *Retinoids: Methods and Protocols*. Humana Press Inc., NJ, USA, Vol. 652, pp. 229–245.
62. Haeseleer, F., Imanishi, Y., Maeda, T., Possin, D.E., Maeda, A., Lee, A., Rieke, F. and Palczewski, K. (2004) Essential role of Ca^{2+}-binding protein 4, a Cav1.4 channel regulator, in photoreceptor synaptic function. *Nat. Neurosci.*, **7**, 1079–1087.